Hydrol. Earth Syst. Sci. Discuss., https://doi.org/10.5194/hess-2018-624
Manuscript under review for journal Hydrol. Earth Syst. Sci.
Discussion started: 8 February 2019

Hydrology and Earth System Sciences
Open Access
Discussions

Steady State Non-isothermal Well Flow in a Slanted Aquifer: Mathematical formulation and Field Application to a Deep Fault in the Xinzhou Geothermal Field in Guangdong, China

Guoping Lu[1*], Bill X. Hu[1*]

[1]Institute of Groundwater and Earth Sciences, Jinan University, 601 Huangpu Avenue West, Guangzhou, Guangdong 510632, China

*Correspondence to: guopinglu@yahoo.com; Tel.: +86-18923379841.
*Correspondence to: bill.x.hu@gmail.com; Tel.: +86-18624375631.

Abstract. This paper develops a novel mathematical formulation for geothermal well flow. Non-isothermal flow would implicate the effectiveness of gravity as a body force term regulated by viscosity and density as well. Consequently it is a critical concept in practice that a dome-shaped water head surface would be present in its equilibrium-state water potential, as a proper observation needed to understand geothermal flow fields. Tabulation and formula are compiled on water density and viscosity as a function of temperatures and pressures to facilitate calculations. The derived formulas were applied to the field study site in a deep fault zone at a geothermal field in coastal Guangdong province, China, based on observations from a thousand-meter-depth borehole drilling project. The deep fault is unique in having a steep plane that emerges at the ground surface, and constitutes fast flow path for deep thermal water up to 115^{o}C and static water pressure up to 10 MPa at the borehole bottom. The fault is conceptualized as an inclined thin aquifer, and formula are derived for thermal outflows for the sloped aquifer to quantify the flow in the fault plane. Results showed that the deep fault has permeability equivalent to clean sands and lower end of unconsolidated gravels. Deep faults could provide useful information on pathways of preferential fluid flows. The deep fault study has several implications in deep geothermal environments and pressure characterizations, regional groundwater circulation limits, and pressure wave propagations in earthquake prediction in the deep crust.

Key words: deep fault, hydraulic conductivity, geothermal flow, slanted aquifer, well flow

1 Introduction

Hydrol. Earth Syst. Sci. Discuss., https://doi.org/10.5194/hess-2018-624
Manuscript under review for journal Hydrol. Earth Syst. Sci.
Discussion started: 8 February 2019

This paper developed mathematical capability to characterize and subsequently discussed its application to the deep fault zone properties in the Xinzhou geothermal field, in coastal Guangdong province of China. The hydraulic property of the deep fault zone were characterized with newly derived formulations for slant aquifer in this paper and based on data from a thousand-meter-deep borehole drilling for the geothermal water flows.

In the Xinzhou geothermal field site, the deep fault plane constitutes the fast flow path of the thermal water. The water temperature is up to 115^{o}C at the borehole water column, with the static water pressure reaching up to 10 MPa at the bottom of the thousand meter borehole. Traditional formulation using the concepts in hydraulic heads is no longer an appropriate independent variable due to the density variant. Another consideration is with dependence of viscosity on temperatures. The research problem faced is how to factor in the buoyancy and viscosity to appropriately characterize the thermal well flow.

Geothermal energy comes in the forms of conductive heat and advective water flow (Bodvarsson and Tsang, 1982). The advective geothermal flow is inherently affected by thermal properties such as lighter density and lower viscosity at elevated temperatures mainly in the form of buoyancy. Geothermal energy is a realistic and emerging source of clean, renewable energy (Baioumy et al., 2015; Regenauer-Lieb et al., 2015; Craig et al., 2013; Younger and Gluyas, 2012; Zhang et al., 2004).

Ground water flows along a fault which is a slant confined fault zone aquifer (Lu et al., 2017; Holland, 2012; Fowles and Burley, 1994). The fault aquifer renders spatial positioning a necessity in quantifying the well flow. Vertical aquifers (Anderson, 2006) is an special case of slanted aquifer. Sloping fault aquifers have additional complexity of flow path in terms of its presentations (Huang et al., 2014; Antonio and Pacheco, 2002). Earlier approach uses a moving boundary to approximate the lowering of the free surface portion of the aquifer from progressive drying up the aquifer during pumping. A mathematical model was later developed for simulating the hydraulic head distribution in response to pumping in a sloping fault zone aquifer under a water table boundary condition (Huang et al., 2014). Analytical solutions of seawater intrusion was developed for sloping confined and unconfined coastal aquifers (Lu et al., 2016). And a semi-analytical solution was presented for groundwater flow due to pumping in a leaky sloping fault-zone aquifer surrounded by permeable matrices (Zhao et al., 2016).

Along the line of aquifer dipping, wedge-shape aquifer was found not able to be estimated by the flow in an aquifer of uniform thickness (Hantush, 1962). Pumping in a sloping unconfined aquifer overlaying a leaky artesian aquifer was studied as a two-dimensional steady-state groundwater well flow (Hantush, 1964). Slant well in horizontal unconfined aquifers was investigated for both instantaneous drainage and delayed yield (Zhan and Zlotnik, 2002). Groundwater flow across an less permeable fault than wall rocks was simulated using simple analytical solutions for steady-state horizontal flow across three domains linked by requiring continuity of head and flux (Haneburg, 1995). All these approaches deal with shallow confined aquifers, which appear limited in thermal effect, and therefore inappropriate for geothermal water flow in deep faults. Deep geothermal water flows are characteristic of elevated temperatures with lighter density and lower viscosity (Xu et al., 2002; Pruess et al., 1999).

In deep faults, the geothermal water is predominantly driven by buoyancy from elevated temperatures. Cumulated effects from lighter density would result in less hydrostatic pressures, inducing thermal waters flowing into the fault zone or fracture zone (Lu et al., 2017). Buoyancy inherent with fluid flows often makes the groundwater emerge as thermal spring up onto the ground surface.

Geothermal waters more likely find their ways through deep faults to flow toward a shallower depth. The temperature effect is pronounced during deep borehole drilling, in which colder circulating drilling water dynamically interacts with the hot geothermal water in surrounding wall rocks (Lu et al., 2017). We want to find out how the temperature effect plays out in the dynamic geothermal water flow to wells of deep fault geothermal field.

In practice the density factor is critical in understanding geothermal flows in a geothermal field. The density factor comes in play as buoyancy force and results in a dome-shaped feature of hydraulic heads. As a result, recognization of this arched head surface is a must to correctly characterize the geothermal flow field, and the fluid flow and interaction of drilling fluids with the thermal waters.

We developed analytical solution to account for the significant temperature effect on the geothermal water flow in the sloping fault zone aquifer, and subsequently applied the well flow equations to the field observation data of the borehole water columns to derive the deep fault permeability data.

Our study is the first of this kind for non-isothermal flows in terms of analytical approach for a slant confined aquifer and its applications to a deep fault. To the best of our knowledge, no relevant analytical equations regarding thermal water flows for fault planes in general field site applications have been found in literatures. Our paper is focused on deep aquifers both with profound thermal effect and fault properties. The research solutions provide tools in quantifying thermal flows and aquifer properties, and the results provide basis and leads to researches on deep thermal and mechanical processes as groundwater circulations and pressure water propagations in the deep crust.

The thermal waters have lower density at a higher temperature as thermal expansion outgains compression in the crust (Pruess et al., 1999). The water density could be slightly affected by the mineral content in salty water and the dissolved gases (Pruess et al., 1999). The geothermal waters tend to get more acidic at an elevated temperature (Lu et al., 2015) at a greater depth.

This paper has several objectives: 1. derivation of an analytical solution for steady radial flow of a borehole for geothermal water in a horizontal aquifer. 2. derivation of analytical solution for radial flow for geothermal water in a dipping aquifer. 3. compilation of density and viscosity data for thermal waters. 4. study of the hydraulic properties of the deep fault in the Xinzhou geothermal field site.

2 Regional Geology and Site Description

2.1 Geological setting

The Xinzhou coastal geothermal field is a part of the coastal China geothermal belt, extending from the south to southeast and continue to east China along the coast. This coastal thermal belt is relayed to the west to the Mediterranean-Himalayas geothermal belt in Yunnan, Tibet, and west Sichuan of southwestern China (Wang et al, 2016; Guo and Wang, 2012; Liao and Zhao, 1999).

Hydrol. Earth Syst. Sci. Discuss., https://doi.org/10.5194/hess-2018-624
Manuscript under review for journal Hydrol. Earth Syst. Sci.
Discussion started: 8 February 2019

Hydrology and Earth System Sciences
Open Access
Discussions

In Guangdong Province, geothermal fields occur in a pattern that reflects the controlling tectonic structures (Figure 1a). Oriented north-south and east-south deep faults are crossed by northeastern strike faults. The Enping-Yangjiang deep fault, located on the western side of the Pearl River estuary, has been observed cut 20 km deep into the crust (Ren et al., 2011).

The study field site is located in the southwestern coastal area in Guangdong province (Figure 1). It is about 19 km away from the coast line and 10 km from the tidal reach of a local river called Shouchang River (Figure 1b). The altitude of Xinzhou geothermal field is about 10 m to 13 m (Figure 1).

Xinzhou geothermal field sees outcrops of Yanshan II granite in the southern and sporadically in the north. The granite forms the northwestern edge of the Xinzhou granite batholith (with an outcrop area of 292.6 km^2). In the Xinzhou basin, the basement rocks are overlain by Quaternary clastic and marine sediments (Figure 1c). At the periphery of the batholith, to the north of the site is the boundary with Precambrian-Cambrian light metamorphic clastic rocks (Figure 1c).

2.2 Xinzhou geothermal field site and drillings

In the Xinzhou field site, hot springs are exposed along the stream bed of the upstream of the coastal Shouchang river (Figure 2). Hot geothermal waters outflow from the earlier drilled boreholes (Figure 2). Hottest 98.4^{o}C outflow (98.4^{o}C) is found in the Jia well located in the middle of the field and the water (Figure 1c).

A deep fault occurs at a high angle (almost vertical at 85^{o}) dipping to the south. The fault was initially revealed in drillings at an earlier time (Liang, 1993), recently further characterized by the geophysical method of Audio Magnetotelluric Sounding (AMT) (Wu, 2013). The faulting is revealed to extend about as deep as 10 km into the crust, based on apparent resistivity and impedance phase surveys (Wang et al., 2015), and confirmed in a 1000-m scientific drilling in 2013 (Wang et al., 2015).

The circulating water column inside a on-going drilling borehole was generally cooler than the borehole wall rocks, creating a higher hydrostatic pressure against the borehole wall. This practically has become a technical utility in overcoming pressurized hot water flowing out of a borehole. Hot water could be triggered to flow out of a borehole when a water-transmitting fault or fracture zone is crossed in drilling. This eruption of flowing hot water comes with an overpressure yields a hydraulic head above the ground surface, which has to be suppressed to order to resume drilling. When down dripping starts, injection of colder drilling water gradually cools the hot water in the borehole, creating a water column of an increasingly higher static pressure and eventually lowering the hydraulic head level to below the ground surface. This effectively suppresses the surging of high-temperature geothermal water. This also serves as the working theory to resume drilling after a thermal eruption, by injecting circulation water into the borehole when starting the down tripping. More and more circulation water into the borehole would eventually lead to suppression of the surging of hot geothermal water.

The borehole temperatures were measured to monitor the thermal gradients for the thousand-meter borehole (Tables 2 and 3; Figure 2). The temperature profiles were characterized before and after the thermal eruption triggered from drilling past the fault plane.

3 Hydraulic properties of geothermal waters

Geothermal waters have variable density and viscosity (Table 1). Generally the density becomes smaller at an elevated temperature (Wagner, 1999; Keenan et al., 1969; and International Formulation Committee, 1967). It is noted that the list is specified for saturated pressures. In comparison, also listed is the density values at pressures of 5 MPa larger over the saturated pressure. The density becomes slightly larger at a higher pressure within the first ten MPa (Table 1).

For a simple calculation, the density can be interpolated from the those listed in Table 1. A more rigorous approach is using numerical calculation of the density value for a pair of given temperature and pressure. In this paper the calculation was also performed using a numerical code modified from the module for density in Tough2 simulator (Pruess et al., 1999). The permeability values reported in Table 2 were computed using the density computed by the revised code. Note that the two methods above yield density values within 0.52% difference and either one is deemed as appropriate.

Viscosity of water is lowered at a higher temperature (Table 1) (Sengers and Watson, 1986). The viscosity fitted for temperatures is good within 0.88% at saturated pressures; and 0.25% at 5 MPa over saturated pressures for temperature between 10-200^{o}C. At 0^{o}C the fit yields under-prediction of the viscosity with error -2.7%, and at 300-350^{o}C has an over-prediction.

Viscosity is affected by pressure in two trends. Higher pressures lead to slightly smaller viscosity for low temperatures (0-25^{o}C), and result in slightly larger viscosity for higher temperatures (around >25^{o}C).

Both water density and viscosity are more subjective to temperature variations and the pressure appears less a factor. For a 5 MPa pressure increase over the saturated pressure, the density gains less than 0.39%, and the viscosity changes less than 0.89% for temperatures in the range of 0-200^{o}C.

Hydrol. Earth Syst. Sci. Discuss., https://doi.org/10.5194/hess-2018-624
Manuscript under review for journal Hydrol. Earth Syst. Sci.
Discussion started: 8 February 2019

The water column will expand and rise to a higher level when being heated up. This explains that an aquifer has a dome shape pressure surface in a geothermal field at steady state condition (Figure 3a).

4 Generalized Darcy's Law

The Darcy's law can be written in the generalized dynamic form as flux in an unit area (Brownell et al., 1977; Hubbert, 1957, 1940):

$$\mathbf{q} = -\mathrm{k}\,\nabla[\frac{1}{\mu}(\mathrm{P}+\rho\mathbf{g}\mathrm{z})] \tag{1a}$$

$$\mathrm{k}\,\nabla[\frac{1}{\mu}(\mathrm{P}+\rho\mathbf{g}\mathrm{z})]+q_s=S_s\frac{\partial \mathrm{P}}{\partial \mathrm{t}} \tag{1b}$$

$$\mathbf{v} = \frac{\mathbf{q}}{\theta} \tag{1c}$$

where $\mathbf{q}$ is the fluid's mass flux vector or called Darcy velocity (kg/m^2/sec), k is the rock permeability (m^2), ρ is the fluid density (kg/m^3) dependent of temperature and pressure (Section 3). μ is kinematic viscosity (m^2/s) dependent of temperature and pressure. Kinematic viscosity μ is related to dynamic viscosity ν (the SI unit, kg/m/s, or Pa s) through $\mu = \nu/\rho$. ∇ is partial derivative respective to coordinates, g is the gravity constant (9.80665 m/s^2), and z is the height relative to a reference point. The negative sign in front of the left side stands for the flow pointing to the opposite of the gradient. v is the average seepage velocity or pore velocity. θ is porosity of the porous medium. q_s is the sink/source term, which is the mass flow rate injected or extracted from unit volume of the aquifer. S_s is specific storage, that is the water amount released from unit volume

Hydrol. Earth Syst. Sci. Discuss., https://doi.org/10.5194/hess-2018-624
Manuscript under review for journal Hydrol. Earth Syst. Sci.
Discussion started: 8 February 2019

Hydrology and Earth System Sciences
Open Access
Discussions

of the aquifer at one unit drop of the head. The pressure P (Pascal in kg/m/s^2) has the form for constant hydrostatic pressure or variable density conditions, respectively:

$$P = \rho g (h - h_0) \tag{2a}$$

$$P = \int_{\rho_0 h_0}^{\rho_m h_m} g \, d(\rho h) \tag{2b}$$

$$P \approx \sum_{i=1}^{m} \rho_i \, g (h_i - h_{i-1}) \tag{2c}$$

where h is the hydraulic head (m), and h_0 is the elevation (m) at a reference point. Summation i for *k*, and *l*, *m*, *n* thereafter are the number of discrete points along the water column.

An useful alternative form of the Darcy's law has the simplified form for groundwater flow:

$$Q = -K \nabla \left(\frac{P}{\rho g} + z \right) \tag{3}$$

where K is called the hydraulic conductivity (m/s), with $K = k g / \mu$ for conversion to permeability. Q is the flux across unit area (m/s, or m^3/m^2/s). Note that strictly Q is volumetric, differing from q in mass (kg/m^2/s), with their conversion $Q = \rho q$.

5. Non-isothermal well flow in a horizontal aquifer and an inclined confined aquifer

Hydrol. Earth Syst. Sci. Discuss., https://doi.org/10.5194/hess-2018-624
Manuscript under review for journal Hydrol. Earth Syst. Sci.
Discussion started: 8 February 2019

5.1 Linear thermal flows in a horizontal aquifer or an inclined confined aquifer

In the geothermal water flow, both fluid density and viscosity are dependent of temperatures. Density affects hydrostatic pressure, and viscosity reflects water's resistance to flow. Assuming that the temperature is linearly varied along the flow direction. In steady state, we have the Darcy's law for the flow in a unit width as:

$$\mathbf{q} = -kM\frac{d}{dl}\left[\frac{1}{\mu}(P + \rho \mathbf{g} z)\right] \tag{4a}$$

$$\frac{\mathbf{q}}{kM}dl = -d\left[\frac{1}{\mu}(P + \rho \mathbf{g} z)\right] \tag{4b}$$

where M is the thickness of the aquifer. l is the length variable. Flow **q** takes positive value for flow opposite to the direction of the length variable. Integration of both sides of Eq.(4b) leads to

$$\mathbf{q}\left(\frac{L_2}{k_2 M_2} - \frac{L_1}{k_1 M_1}\right) = -\int_{L_1}^{L_2} d\left(\frac{P}{\mu}\right) - \int_{L_1}^{L_2} d\left(\frac{\rho \mathbf{g} z}{\mu}\right) \tag{5a}$$

$$\mathbf{q}\left(\frac{L_2}{k_2 M_2} - \frac{L_1}{k_1 M_1}\right) = -\left(\frac{P}{\mu}\right)\Big|_{L_1}^{L_2} - \left(\frac{\rho \mathbf{g} z}{\mu}\right)\Big|_{L_1}^{L_2} \tag{5b}$$

where L is length along the flow, with subscripts 1 and 2 indicate variable at the starting point and ending point, respectively. The summation terms are referred to Eq. (2c). The pressure term can be calculated accurately or approximated by Eq. (2b,c) for the water column revealed in a borehole. The second term on the right-hand side is the additional term for gravity as a body force exerting on the system, arising from elevation difference and compounded by the thermal effect in terms of density and viscosity. The elevation reference point is set to either one of the calculation points, in order to yield a correct body force term owing to an elevation difference.

5.2 Non isothermal radial flow in a horizontal confined aquifer

Assuming in a horizontal confined aquifer, in the non-isothermal scenario, fluid density and viscosity are variables of temperature (Figure 4c). The flow to the pumping well can be obtained from Eq. (1a) by accounting flow area in the radial domain:

$$q_w = 2\pi k M r \frac{d}{dr}\left(\frac{1}{\mu}(P + \rho g h)\right) = 2\pi k M r\left[\frac{d}{dr}\left(\frac{P}{\mu}\right) + \frac{d}{dr}\left(\frac{\rho g h}{\mu}\right)\right] \tag{6}$$

where q_w is the flow rate (m^3/s). It is assumed that P is constant over time. With the assumption of elevation z independent of locations, the second term on the right-hand side vanishes because no elevation difference in a horizontal aquifer.

Integrations of pressure and density, as well as viscosity, over the radial lead to

$$\int_r \frac{q_w}{2\pi k M r} dr = \int_\mu d\left(\frac{P}{\mu}\right) + \int_{h,\rho,\mu} d\left(\frac{1}{\mu}\rho g h\right) \tag{7}$$

Both sides can be integrated as

$$\frac{q_w}{2\pi k M}\ln(r_2/r_1) = \frac{P}{\mu}\Big|_{R_2} - \frac{P}{\mu}\Big|_{R_1} \tag{8a}$$

$$\frac{q_w}{2\pi k M}\ln(r_2/r_1) = \frac{1}{\mu}\rho g h\Big|_{H_2}^{H_{T2}} - \frac{1}{\mu}\rho g h\Big|_{H_1}^{H_{T1}} \tag{8b}$$

$$\frac{q_w}{2\pi k M}\ln(r_2/r_1) = \sum_{i=1}^{m}\frac{1}{\mu_i} g \rho_i h_i\Big|_{R_2} - \sum_{i=1}^{n}\frac{1}{\mu_i} g \rho_i h_i\Big|_{R_1} \tag{8c}$$

Hydrol. Earth Syst. Sci. Discuss., https://doi.org/10.5194/hess-2018-624
Manuscript under review for journal Hydrol. Earth Syst. Sci.
Discussion started: 8 February 2019

where subscript R_1 and R_2 marking the location of the boreholes, subscript H indicating height, subscripts 1 and 2 for locations at borehole locations x2 and x1 in the aquifer, and subscript T for the top of the borehole water column. The pressure terms are determined by the correspondent borehole's water column, which has temperature dependent density and viscosity.

The water potential term is reversely proportional of the kinematic viscosity (momentum diffusivity) as the resistance of water flow. As the viscosity becomes smaller at a higher temperature, the water potentials lead to a net loss for an elevated temperature around the pumping well; on the other hand, it results to a net gain for an abated temperature at the pumping well. Eq.(16a,b) is reduced to the general case of flow in a horizontal confined aquifer as in Eq.(7) for no variations in density and viscosity

5.3 Non isothermal flow in an inclined confined aquifer

Considering the non-isothermal scenario, both fluid density and viscosity are variables. In a dipped confined aquifer (Figure 4d), the flow to the pumping well can be obtained from Eq. 1a, by accounting flux face in the radial domain:

$$q_w = 2\pi k M r \frac{d}{dr}\left[\frac{1}{\mu}(P + \rho \mathbf{g} z)\right] = 2\pi k M r \frac{d}{dr}\left[\frac{1}{\mu}\rho g (h + z)\right] \tag{9a}$$

$$E = E_0 + z = E_0 + A x \tag{9b}$$

$$r^2 = x^2 + y^2 + z^2 = (1 + A^2) x^2 + y^2 \tag{9c}$$

Hydrol. Earth Syst. Sci. Discuss., https://doi.org/10.5194/hess-2018-624
Manuscript under review for journal Hydrol. Earth Syst. Sci.
Discussion started: 8 February 2019

where the r is defined in Eq. (9c). z is the elevation of the sloped aquifer, and can be related to x a line through the origin (Figure 4c), defined by $z = A\,x$ at the well through the aquifer , with E being the elevation, E_0 as elevation at origin (0, 0), and A as the slope.

Substituting Eqs. (9b,c) into Eq. (8) leads to

$$d(\frac{1}{\mu}P) + d(\frac{1}{\mu}\rho g z) = \frac{Q_w}{2\pi k M}\frac{x\,dx + y\,dy + z\,dz}{r^2} \tag{10a}$$

$$d(\frac{1}{\mu}\rho g h) + d(\frac{1}{\mu}\rho g z) = \frac{Q_w}{2\pi k M}\frac{(x + A^2 x\ )dx + y\,dy}{(1 + A^2)x^2 + y^2} \tag{10b}$$

Integration over both sides have

$$\frac{1}{\mu}\rho g h + \frac{1}{\mu}\rho g A x = \frac{Q_w}{4\pi K M}\ln[(1 + A^2)x^2 + y^2] + C \tag{10c}$$

Integrating over radius R_1 to R_2, with corresponding x_1 to x_2, leads to:

$$\frac{1}{\mu}\rho g h\Big|_{H_2}^{H_{T2}} - \frac{1}{\mu}\rho g h\Big|_{H_1}^{H_{T1}} + \frac{1}{\mu}\rho g A x_2\Big|_{H_0}^{H_{H_2}} - \frac{1}{\mu}\rho g A x_1\Big|_{H_0}^{H_{H_1}} = \frac{q_w}{4\pi k M}\ln\frac{(1 + A^2)x_2^2 + y_2^2}{(1 + A^2)x_1^2 + y_1^2} \tag{11a}$$

Hydrol. Earth Syst. Sci. Discuss., https://doi.org/10.5194/hess-2018-624
Manuscript under review for journal Hydrol. Earth Syst. Sci.
Discussion started: 8 February 2019

$$\begin{aligned}&\sum_{i=1}^{k}\frac{1}{\mu_i} g\rho_i h_i|_{R_2} - \sum_{i=1}^{l}\frac{1}{\mu_i} g\rho_i h_i|_{R_1} + \\ &\quad\sum_{i=1}^{m}\frac{1}{\mu_{x_2}}\rho_{x_2} gAx_2|_{H_0\to H_2} - \sum_{i=1}^{n}\frac{1}{\mu_{x_1}}\rho_{x_1} gAx_1|_{H_0\to H_1} \\ &= \frac{q_w}{4\pi kM}\ln\frac{(1+A^2)x_2^2+y_2^2}{(1+A^2)x_1^2+y_1^2}\end{aligned} \tag{11b}$$

where subscript H indicates height, subscripts 1 and 2 for locations at borehole locations x2 and x1 in the fault plane, subscript 0 for the elevation reference point (which could be set at where the borehole crossing the fault aquifer plane for simplified calculation), and subscript T for the top of the borehole water column. The 3rd and 4th terms on the left-hand side are for the gravity terms from reference point H_0 to H_2, H_0 to H_1, respectively. The above formula would reduce to simplified scenario of isothermal radial flow in Eq. (13) below.

A general equation for thermal flow in an irregular fault plane can be written as

$$\begin{aligned}&\frac{1}{\mu}\rho g\, h|_{H_2}^{H_{T2}} - \frac{1}{\mu}\rho g\, h|_{H_1}^{H_{T1}} + \frac{1}{\mu}\rho g\, H|_{H_0}^{H_{H_2}} - \frac{1}{\mu}\rho g\, H|_{H_0}^{H_{H_1}} \\ &= \frac{q_w}{4\pi k M}\ln\left(\frac{r_2^2}{r_1^2}\right)\end{aligned} \tag{12a}$$

$$\begin{aligned}&\sum_{i=1}^{k}\frac{1}{\mu_i} g\rho_i h_i|_{x_2} - \sum_{i=1}^{l}\frac{1}{\mu_i} g\rho_i h_i|_{x_1} + \\ &\quad\sum_{i=1}^{m}\frac{1}{\mu_{x_2}}\rho_{x_2} gH|_{H_0\to H_2} - \sum_{i=1}^{n}\frac{1}{\mu_{x_1}}\rho_{x_1} gH|_{H_0\to H_1} \\ &= \frac{q_w}{4\pi kM}\ln\left(\frac{r_{x_2}^2}{r_{x_1}^2}\right)\end{aligned} \tag{12b}$$

where the summations are calculations of the pressure exerted to the point x_1 or x_2 in the fault plane by the water column in the borehole, index *i* for numbering temperature measurement points, with *k* or *l* for total number of points of observed temperatures. The r's take the distance along the path on the irregular plane.

The corresponding isothermal equation can be written for an irregular fault plane, given that one knows the distances r_1 and r_2 (from the well) and the heights h_1 and h_2 for two observation points.

$$(s_1 - s_2) + (h_2 - h_1) = \frac{Q_w}{8\pi K M} \ln\left(\frac{r_2^2}{r_1^2}\right) \qquad (13)$$

And this reduces to the commonly seen Thiem equation with the h terms cancelled out when the slope of the aquifer plane is zero (Bear, 1972).

6. Application to hydraulic dynamics of a deep fault

We used the deep fault in Xinzhou geothermal field to study the hydrodynamics of the fault zone. The Xinzhou geothermal field shows a dome-shape potential surface for the geothermal water in the early exploration in 1983 (Liang, 1993). The flow field can be considered at equilibrium state in terms of the geothermal flows of heat and water.

The Xinzhou deep fault is an high dip-angle fault that extends thousand meters deep into the crust (Lu et al., 2017; Wang et al., 2015). A thousand-meter borehole was able to penetrate the fault plane (Figure 1). There had been several existent boreholes prior to the drilling of the thousand borehole.

Well boreholes had been drilled on the hanging wall of the deep fault before the thousand meter borehole. Ta well penetrated the fault plane at the depth of 220 m. The deep fault outcrops at the eastern end at Maoshui Pool, in which geothermal water oozes from the fault down under.

The deep fault system is set to have a reference point at the penetrated spot by the thousand meter borehole (Figure 5). The x-axis points eastward parallel to the fault plane

Hydrol. Earth Syst. Sci. Discuss., https://doi.org/10.5194/hess-2018-624
Manuscript under review for journal Hydrol. Earth Syst. Sci.
Discussion started: 8 February 2019

Hydrology and Earth System Sciences
Open Access
Discussions

and the y-axis is horizontally pointing to the footwall. A cross section of the aquifer is shown in Figure 5b. The data for the calculations are listed in Table 2.

In the calculations the boreholes used were the ones that across the deep fault plane (Table 2). The only exception was Jia well, which was not deep enough to penetrate the fault plane. It is close to the fault and has well fractured wall rocks as flow paths (Lu et al., 2017). It is believed to have been well connected to the fault plane.

The water columns inside the boreholes were used to calculate the pressure head $\sum_{i}\frac{1}{\mu_i} g\rho_i h_i$ at the point crossing the fault plane. Those boreholes shallower than the thousand-meter borehole need to calculate the height interval Hi (from the fault layer middle point at the borehole to the reference point at the thousand-meter borehole) for the term $\sum_{i=1}^{m}\frac{1}{\mu_i} g\rho_i A x|_{(x_2)}$. The calculations were based on density and viscosity data corresponding to the linearly interpreted temperature data and coordinate data (Tables 1 and 2).

In the calculation of the water density, the effect of salts and dissolved gases on the water density was assumed to be minimal and thus be neglected. This assumption is based on the dilute nature and lack of gassy content in the thermal waters in the field site. And this is believed to have negligible effect on the accuracy on resultant calculated values, considering temperature being of dominant controlling factor.

The calculated permeability values for the deep fault are on the scale of 1.0e-11 m^2 (Table 2). And the fault plane is approximated to be homogenous with a thickness of 1 m, based on the thousand-meter borehole drill core and historical data for the previous drilling. In the calculation, we assume that the fault has a much larger permeability than the fault wall rocks.

7. Discussions and Implications

7.1 Borehole hydraulic dynamic causing water flow to higher ground

Thermal effect has showed the dynamic of the geothermal flow system. In the thousand meter borehole drilling, relatively higher pressure head was created by the relatively colder circulating drilling fluids (Table 3). After the drilling has reached a certain depth, the drilling operation had paused for several days for thermal recovery prior to temperature profile measurement.

After stoppage of the drilling for temperature profile measurements, the thermal recovery was progressively having made the water level rising in the borehole (Table 3). The arising borehole water level eventually reached the top the borehole and caused eruption of the thermal flow.

A relatively lower pressure head was created in the initial stage of the thermal recovering stage, followed by a gradually increasing head level (Table 3, Figure 3). The pressures evolve from initial thermal recovery stage to the eventual outflowing during the thermal recovery, demonstrating the borehole flow field reversal from colder drilling water and hotter geothermal water.

In the processing of drilling the drilling fluid cooled down the borehole and subsequently the wall rocks. The cooler circulated water column in the borehole created greater pressure head than that at hotter water. The drilling water flowed outward to the fault zone aquifer and the fault wall rocks, creating a leaky condition. This has been interesting that the drilling water had been observed to have flowed from the lower ground at the drilling platform flow to the Ta well (7.1 m above the ground, Table 2). This is evident that the lubricant in drillings was found and shown up as oil sheen in other thermal well flows.

7.2 Extremely large permeability of the fault zone aquifer and implications

The calculated permeability values (3.29e-11 to 1.06e-10 m^2) (Table 2) are equivalent to the median ones of unconsolidated clean sand which is in the range of 1.0e-13 to 1.0e-9 m^2 (Freeze and Cherry, 1979). And it is at the lower end of unconsolidated gravel (1.0e-10 to 1.0e-7 m^2) (Freeze and Cherry, 1979).

The fault permeability obtained in this study is very close to but a little larger than the value of 1.3e-12 m^2 derived from large scale simulation in Lu et al. (2017). The somewhat smaller permeability from the earlier simulation approach might result from the relatively course resolution of the discretization, in which the thermal vent was approximated as one borehole.

We assume that the fractured walls of the fault would not alter the basic fast flow pattern in the fault zone. This is based on the observation that the well boreholes drilled within the hanging wall or footwall have much small flow rates than those crossing the fault plane (Figure 1). The wells drilled into the fractured wall rocks include Xiting well, Dun well, Old hole and East Tang wells. They have relatively small flow rates below 1.0 L/s. Above all, the fault flow is diverted into rocks of the fractured walls rather than

Hydrol. Earth Syst. Sci. Discuss., https://doi.org/10.5194/hess-2018-624
Manuscript under review for journal Hydrol. Earth Syst. Sci.
Discussion started: 8 February 2019

Hydrology and Earth System Sciences
Open Access
Discussions

being draining by the latter. We could conclude that the calculated permeability numbers from well hydraulics are served as the lower limit defining the fault's properties.

The high permeability values of the fault zone aquifer is seemingly directly related to fast flow path of geothermal waters. This has several potential implications. Our results for the fault permeability could also be valid to the deeper portion of the deep fault. The geothermal reservoir in the Xinzhou field is estimated at around 3,500 m depth, which is linked to the borehole through the fault plane (Lu et al., 2017). The high permeability of the fault zone indicates that the deep fault zones could have deep underground environmental conditions favoring pressure wave propagation (Yang et al., 2015; Silin et al., 2003). And the fast flow path in the deep crust could favor the porosity wave propagation (Rass et al., 2018; Yarushina et al., 2015).

Another potential implication involves deep groundwater circulations through deep faults. The fast flow paths in deep faults could channel deep geothermal waters toward shallower depths, creating a relatively lower pressure zone in the deep underground. Deep groundwater in wall rocks is thus favored to flow toward the fault aquifer, forming deeper circulating groundwater. This could significantly deepen the circulation limits of regional groundwater.

8. Conclusions

In a geothermal field the water density factor plays an important role in understanding the flow field. The equipotential surface presents itself as a dome-shaped hydraulic head surface.

Hydrol. Earth Syst. Sci. Discuss., https://doi.org/10.5194/hess-2018-624
Manuscript under review for journal Hydrol. Earth Syst. Sci.
Discussion started: 8 February 2019

We have developed a series of analytical solutions for non-isothermal geothermal steady-state water flows to wells in a confined aquifer with horizontal and dipped layer planes. Necessary density and viscosity data were compiled for temperatures at saturated pressures, with additional density data at higher pressures.

The analytical approach is useful in this case because it can accommodate dipped aquifer or dipped fault plane under non-isothermal condition rather than the horizontal aquifer for isothermal case. The temperature effect is accounted for through water density and viscosity.

In thermal flows, gravity as a body force term has a varied effectiveness on driving the flow because it would be regulated by viscosity and density as well. In other words, gravity affects thermal flow differentially with variations in viscosity and density (equation of state).

Our findings showed that the deep fault in the Xinzhou geothermal field has a large permeability at the scale of 1.0e-11 m^2. This fault property corresponds to that of clean sands and the lower end of gravels.

The primary uncertainties in relating calculations to the real world is the steady-state nature of the formulation. An field application is involved with thickness of the fault zone, which may vary from place to place.

Our work represents the first study with analytical solution approach for field study of a deep fault zone. It provides a basis for further studies of deep fault property. The results bear implications in propagation of porosity waves and regional groundwater's deep circulations in the deep crust by geothermal waters under higher temperatures in the crust.

Acknowledgments

This study was financially supported by the National Natural Science Foundation of China (NSFC) Grant (No.41572241), and partially by The startup fund for teacher by Jinan University. Special thanks to the help from Guangdong Provincial Hydrogeology Brigade for access to unpublished data and assistance with field works. We are grateful to the editors and the reviewers for the comments to improve the manuscript.

References

Anderson, E.I.: Analytical solutions for flow to a well through a fault, Adv. Water Resour., 29 (12), 1790–1803, 2006. http://dx.doi.org/10.1016/j.advwatres.2005.12.010.

Antonio, F., and Pacheco, L.: Response to pumping of wells in sloping fault zone aquifers, J. Hydrol., 259 (1–4), 116–135, 2002.

Baioumy, H., Nawawi, M., Wagner, K., and Arifin, M.H.: Geochemistry and geothermometry of non-volcanic hot springs in West Malaysia, J. Volcanol. Geoth. Res., 290, 12-22, 2015.

Bear, J.: Dynamics of Fluids in Porous Media, Dover, Mineola, N. Y., 1972.

Beaude, L., Brenner, K., Lopez, S., Masson, R., and Smai, F.: Non-isothermal compositional liquid gas Darcy flow: formulation, soil-atmosphere boundary condition and application to high energy geothermal simulations. 2018. <hal-01702391>

Birhanu, Z.K., Nils-Otto Kitterod, Krogstad, H., and Kvarno, A.: Analytical and Numerical Solutions of Radially Symmetric Aquifer Thermal Energy Storage Problems, Hydrol. Earth Syst. Sci. Discuss., https://doi.org/10.5194/hess-2017-303, 2017.

Bodvarsson, G.S., Tsang, C.F.: Injection and thermal breakthrough in fractured geothermal reservoirs. Journal of Geophysical research Atmospheres 87(B):1031-1048, 1982.

Bredehoeft, J.D.: Fault permeability near Yucca Mountain, Water Resour. Res., 33(11), 2459–2463, 1997. http://dx.doi.org/10.1029/97wr01710.

Brownell, D.H., Garg, S.K., Pritchett, J.W.: Governing equations for geothermal reservoirs, Water Resour. Res., 13 (6), 1977.

Craig, J., Absar, A., Bhat, G.M., and Thusu, B: Hot springs and the geothermal energy potential of Jammu & Kashmir State, N.W. Himalaya, India. Earth-Sci. Rev., 126, 156-177, 2013. DOI: 10.1016/j.earscirev.2013.05.004.

Fowles, J., and Burley, S.: Textural and permeability characteristics of faulted, high-porosity sandstones, Mar. Petrol. Geol., 11(5), 608–623, 1994.

Freeze, R.A., and Cherry, J.A.: Groundwater. Prentice-Hall, Inc., Englewood Cliffs, 1979.

Gudmundsson, A., Berg, S.S., Lyslo, K.B., Skurtveit, E.: Fracture networks and fluid transport in active fault zones, J. Struct. Geol., 23 (2–3), 343–353, 2001.

Guo, Q. H., and Wang, Y.X.: Geochemistry of Hot Springs in the Tengchong Hydrothermal Areas, Southwestern China. Journal of Volcanology and Geothermal Research, 215, 61–73, 2012

Haneberg, W.C.: Steady-state groundwater-flow across idealized faults, Water Resour. Res., 31 (7), 1815–1820, 1995.

Hantush, M.S.: Flow of ground water in sands of nonuniform thickness. 1. Flow in a wedge-shaped aquifer, J. Geophys. Res., 67(2), 703, 1962.

Holland, M.: Evaluation of factors influencing transmissivity in fractured hard-rock aquifers of the Limpopo Province, Water SA, 38 (3), 2012, http://dx.doi.org/10.4314/wsa.v38i3.3.

Huang, C.-S., Yang, S.-Y., and Yeh, H.-D.: Groundwater flow to a pumping well in a sloping fault zone unconfined aquifer, Water Resour. Res., 50, 4079–4094, 2014, doi:10.1002/2013WR014212.

Hubbert, M.K.: The theory of ground water motion, J. Geol, 48(8), 785-944, 1940.

Hubbert, M.K.: Darcy's Law and the field equations of the flow of underground fluids, International Association of Scientific Hydrology. Bulletin, 2:1, 23-59, 1957. DOI: 10.1080/02626665709493062.

International Formulation Committee: A Formulation of the Thermodynamic Properties of Ordinary Water Substance, IFC Secretariat, Düsseldorf, Germany, 1967.

Johnson, R.B., and DeGraff, J.V.: *Principles of Engineering Geology*, Wiley, 1988.

Keenan, J. H., Keyes, F.G., and Hill, P.G.: Steam tables: Thermodynamic properties of 18 water including vapor, liquid, and solid phases (International System of Units-S.I.). Wiley, New York. pp.162, 1969.

King, C. Y.: Gas Geochemistry Applied to Earthquake Prediction: An Overview. Journal of Geophysical Research, 91: 12269–12281, 1986.

Liang, C.S.: Geochemical characteristics of Xinzhou geothermal field, Guangdong Province. Guangdong Geology, 8 (3), 55-61, 1993. (in Chinese).

Liao, Z., Zhao, P: Yunnan-Tibet Geothermal Belt-Geothermal Resources and Case Histories. Science Press, Beijing, 1999. (in Chinese with English Abstract).

Lide, D.: CRC Handbook of chemistry and physics, 84th edition, 2003-2004. CRC press, LLC, 2002.

Lu, C., Xin, P, Kong, J., Li, L., and Luo, J.: Analytical solutions of seawater intrusion in sloping confined and unconfined coastal aquifers, Water Resour. Res., 52, 6989-7004, 2016. doi:10.1002/2016WR019101.

Lu, G., Wang, X, Xu, F., Li, F., Wang, Y., Qi, S., Yuen, D.: Deep geothermal processes act through deep fault and solid tide in Xinzhou geothermal field in coastal Guangdong, China, Physics of the Earth and Planetary Interiors, 264, 76–88, 2017, http://dx.doi.org/10.1016/j.pepi.2016.12.004.

Lu, G., and Liu, R: Aqueous chemistry of typical geothermal springs with deep faults in Xinyi and Fengshun in Guangdong Province, China. Journal of Earth Science 26, 060-072, 2015.

Lu, G., and Zhang, D.: Nonstationary stochastic analysis of flow in a heterogeneous semiconfined aquifer, Water Resour. Res., 10.1029/2001WR000546, 38(8), 30-1~11, 2002.

Pruess, K., Oldenburg, C.M., and Moridis, G.: TOUGH2 User's Guide. Report LBNL-43134, 1999. Lawrence Berkeley National Laboratory, Berkeley, CA.

Räss, L., Simon, N. S. C., and Podladchikov, Y. Y.: Spontaneous formation of fluid escape pipes from subsurface reservoirs, Nature, 8, 11116, 2018, DOI:10.1038/s41598-018-29485-5

Regenauer-Lieb, K., Yuen, D. A., Qi, S.H., et al.: Forward: Toward a Quantitative Understanding of the Frontier in Geothermal Energy. Journal of Earth Science, 26(1), 1, 2015. doi:10.1007/s12583-015-0601-4

Ren, Z.H., Ye, X.W., and Wei, M.C.: Deep fault distribution interpreted by gravity data in the Pearl River Delta Region, Earthquake Research in Sichuan, 04, 29-34, 2001 (in Chinese)

Sengers, J.V., and Watson, J.T.R.: Improved international formulations for the viscosity and thermal conductivity of water substance, J. Phys. Chem. Ref. Data, 15, 1291, 1986.

Silin, D., Korneev, V., and Goloshubin, G.: Pressure diffusion waves in porous media, Report No.: LBNL--52536-Ext.-Abs.article, April 8, 2003; Berkeley, California. (digital.library.unt.edu/ark:/67531/metadc735497/: accessed June 5, 2018), University of North Texas Libraries, Digital Library, digital.library.unt.edu; crediting UNT Libraries Government Documents Department.

Sun, D.M., and Zhan, H.B.: Flow to a horizontal well in an aquitard–aquifer system, J. Hydrol., 321 (1–4), 364–376, 2006.

Wagner, W.: The IAPWS formulation 1995 for the thermodynamic properties of ordinary water substance for general and scientific use, Journal of Physical and Chemical Reference Data, 31(2), 387, 1999.

Wang, X., Lu, G., and Hu, B.X.: Hydrogeochemical characteristics and geothermometry applications of thermal waters in coastal Xinzhou and Shenzao Geothermal Fields, Guangdong, China, Geofluids, vol. 2018, Article ID 8715080, 24 pages, 2018. doi:10.1155/2018/8715080.

Wang, P., Chen, X., Shen, L., Wu, K., Huang, M., and Xiao, Q.: Geochemical features of the geothermal fluids from the Mapamyum non-volcanic geothermal system (Western Tibet, China), Journal of Volcanology and Geothermal Research, 320, 29-39, 2016.

Wang, Y.X., Du, H.Y., Qi, S.H. et al.: The Geothermal and heat controlling geostructures for Pearl River Delta and periphery, China Geological Survey Report, 2015.

Yang, D., Li, Q. and Zhang, L.: Propagation of pore pressure diffusion waves in saturated porous media. Journal of Applied Physics 117, 134902, 2015. https://doi.org/10.1063/1.4916805. https://aip.scitation.org/doi/full/10.1063/1.4916805

Younger, P.L., and Gluyas, J.G.: Development of deep geothermal energy resources in the UK, Proc. Inst. Civ. Eng.-Energy, 165 (1), 19-32, 2012.

Yarushina, V.M., Podladchikov, Y.Y., Connolly, J.A.D.: (De)compaction of porous viscoelastoplastic media: Solitary porosity waves, J. Geophys. Res. Solid Earth 120, 2015. http://dx.doi.org/10.1002/2014JB011260.

Zhan, H.B. , and Zlotnik, V.A.: Groundwater flow to a horizontal or slanted well in an unconfined aquifer, Water Resour. Res. 38 (7), 1108,2002.

Hydrol. Earth Syst. Sci. Discuss., https://doi.org/10.5194/hess-2018-624
Manuscript under review for journal Hydrol. Earth Syst. Sci.
Discussion started: 8 February 2019

Hydrology and Earth System Sciences Discussions
Open Access

Zhao, Y., Zhang, Y.-K., and Liang, X.: Analytical solutions of three-dimensional groundwater flow to a well in a leaky sloping fault-zone aquifer, Journal of Hydrology, 539, 204-213, 2016. http://dx.doi.org/10.1016/j.jhydrol.2016.05.029.

Hydrol. Earth Syst. Sci. Discuss., https://doi.org/10.5194/hess-2018-624
Manuscript under review for journal Hydrol. Earth Syst. Sci.
Discussion started: 8 February 2019

Tables and Figures

Table 1 Density and viscosities of water

T(°C)[a]	Saturated Pressure (MPa)	Density[a] (kg/m^3)	Dyn. Viscosity[b,c] mPa s	Kin.Viscosity $m^2/s \times 10^6$	Pressure (MPa)	Density[b] (kg/m^3)	Dyn. Viscosity[,c] mPa s	Kin.Viscosity $m^2/s \times 10^6$
0	0.1	999.84	**1.793**	1.793	5.1	1002.35	**1.7807**	1.7765
10	0.1	999.70	**1.307**	1.307	5.1	1002.04	1.2923	1.2897
20	0.1	998.21	**1.002**	1.004	5.1	1000.46	1.0008	1.0003
25	0.1	997.05	**0.8905**	0.8931	5.1	999.27	**0.8889**	0.8895
30	0.1	995.65	**0.7977**	0.8012	5.1	997.84	0.7992	0.8009
40	0.1	992.22	**0.6532**	0.6583	5.1	994.38	0.6548	0.6585
50	0.1	988.03	**0.5470**	0.5536	5.1	990.19	**0.5477**	0.5531
60	0.1	983.20	**0.4665**	0.4745	5.1	985.35	0.4672	0.4741
70	0.1	977.78	**0.4040**	0.4132	5.1	979.94	0.4045	0.4128
80	0.1	971.82	**0.3544**	0.3647	5.1	974.00	0.3549	0.3644
90	0.1	965.35	**0.3145**	0.3258	5.1	967.57	0.3150	0.3256
100	0.1	958.40	**0.2818**	0.2940	5.1	960.67	**0.2831**	0.2947
110	0.1434	950.98	0.2526	0.2656	5.1434	953.34	0.2555	0.2680
120	0.1988	943.08	0.2302	0.2441	5.1988	945.58	0.2329	0.2463
130	0.2704	934.8	0.2112	0.2259	5.2704	937.37	0.2133	0.2276
140	0.3617	925.9	0.1951	0.2107	5.3617	928.78	0.1975	0.2126
150	0.4763	916.7	**0.1825**	0.1991	5.4763	919.78	**0.1837**	0.1997
160	0.6180	907.1	0.1691	0.1864	5.6180	910.36	0.1713	0.1882
170	0.7331	897.3	0.1586	0.1768	5.7331	900.48	0.1607	0.1785
180	1.0030	887.0	0.1493	0.1683	6.0030	890.25	0.1513	0.1700
190	1.2555	876.3	0.1411	0.1610	6.2555	879.54	0.1430	0.1626
200	1.5552	865.0	**0.1344**	0.1554	6.5552	868.35	**0.1356**	0.1562
225	2.5498	834.0	0.1187	0.1423	7.5498	838.23	0.1202	0.1434
250	3.9766	798.6	**0.1061**	0.1329	8.9766	804.47	**0.1075**	0.1336
275	5.9465	758.6	0.0976	0.1287	10.9465	764.54	0.0988	0.1292
300	8.5885	712.5	**0.08592**	0.1206	13.5885	722.39	**0.08782**	0.1216
325	12.0509	654.9	0.07600	0.1160	17.0509	671.01	0.07913	0.1179
350	16.5305	572.8	**0.06609**	0.1154	21.5305	607.59	**0.07045**	0.1159

Note: a. At saturated pressure (Wagner, 1999), critical point at 647.096K, 22.064 MPa density 322 kg/m^3. b. Viscosity in bold is from Sengers and Watson (1986) and Lide (2002), c. Dynamic viscosity calculated for (Pa s or kg/m/s) $\nu = A \times 10^{B/(D\times T-C)}$ for the temperature range (0-250°C), where T is temperature in Kelvin, for saturated pressure A = 2.4×10^{-5} Pa·s, B = 246 K, and C = 140 K, D=0.995; for pressure 5 MPa above the saturated pressure $A = 2.4\times10^{-5}$ Pa·s, B = 257.62 K, C= 140 K, and D = 1.02.

Hydrol. Earth Syst. Sci. Discuss., https://doi.org/10.5194/hess-2018-624
Manuscript under review for journal Hydrol. Earth Syst. Sci.
Discussion started: 8 February 2019

Table 2 Well Borehole data and calculated permeability values for the deep fault at Xinzhou geothermal field[a,b,c]

No.	Well borehole	x(m)	y (m)	Borehole Ground Elevation (m)	Head above ground[b] (m)	T^d (^oC)	Outflow (10^3 kg/d)
1	Maoshui Pool	316.2	67	7.75	1.0	66.5/66.5(0)	120
2	Dongwei Well	324.5	64.75	9.0	-0.25	71.0/88(23)	0
3	Jia Well	10.0	44.0	7.9	4.2	98/98(22)	550
4	Ta Well	-8.0	53	8.15	7.1	96/101(160)	350
5	1000 m well borehole[f]	0.0	0.0	7.8	0	95/107(740)	850
6	F1 Fault[g]	-	67				

No.	Well borehole	P^e (MPa)	$\sum \rho g h/\mu^f$	k (m^2)[h]
1	Maoshui Pool	7.081	2.66E+07	1.06e-10
2	Dongwei Well	7.067	2.96E+07	3.29e-11
3	Jia Well	7.059	3.16E+07	2.15e-11
4	Ta Well	7.097	3.17E+07	2.16e-11
5	1000 m well borehole[g]	7.055	2.52E+07	-
6	F1 Fault[h]			1.3e-12[i]

Note: a. Basic data records refer to site report (Wang et al., 2015; Liang, 1993). b. Pressure calculated for what above the 740 m depth of the 1000 m well. c. The deep fault dips southward at an angle of 85^o. d. Temperature at the top/bottom (depth at the fault plane in parenthesis) of the borehole water column. e. Hydrostatic water pressure of each borehole relative to the point of 1000-m-borehole intercepting the fault plane. f. Hydrostatic pressure term with viscosity effect for the water column above reference point of the 740 m depth. g. Borehole drilling started Oct.1, 2013. Burst Outflow 850 m^3/day at 19:30 on Nov. 7, 2013, borehole diameter 0.15 m. Temperature measurements shown in Figure 2. h. Calculations using Eq. (11b), with approximation the fault zone plane as 1 m. i. Source from Lu et al. (2017).

Hydrology and Earth System Sciences
Open Access
EGU
Discussions

Table 3. Temperature measurements for the 1000 m depth borehole[a,b,c]

Well borehole	Head above ground (m)	T^d (°C)	$P^{c,e}$ (MPa)	Outflow (10^3 kg/d)
A1(685m) 10/30	-2.2	37.0~99.2	6.580	993.4~961.7
A2 (685m) 10/31	-1.5	42.8~102.0	6.561	991.9~959.8
A3(685m) 11/01	-0.45	45.0~104.5	6.550	990.3~957.9
A4(685m) 11/02	-0.35	51.9~106.8	6.538	987.2~956.2
B(740m) 11/09 (outflow)	+5.5	97.9~109.8	6.996	959.6~954.2
C(1002m) 12/07	-1.5	35.1~96.7	7.087	994.1~963.8
C f(1002m) 12/07	+5.5	98.0~113.0	7.055	959.6~954.8

Note: a. Basic data records refer to the site report (Wang et al., 2015; Liang, 1993). b. Pressure calculated for water above 740 m depth; The deep fault dips southward at angle of 85°. c. The drilling fluid at temperature around 45°C, having pressure of 7.180 MPa at the reference point at which borehole crossing the fault plane. d. Temperatures at the top and bottom of the borehole water column. e. Borehole water pressure at the point (depth 740 m) intercepting the fault plane. Temperature measurements shown in Figure 2.

Hydrol. Earth Syst. Sci. Discuss., https://doi.org/10.5194/hess-2018-624
Manuscript under review for journal Hydrol. Earth Syst. Sci.
Discussion started: 8 February 2019

Hydrology and Earth System Sciences
Open Access
Discussions

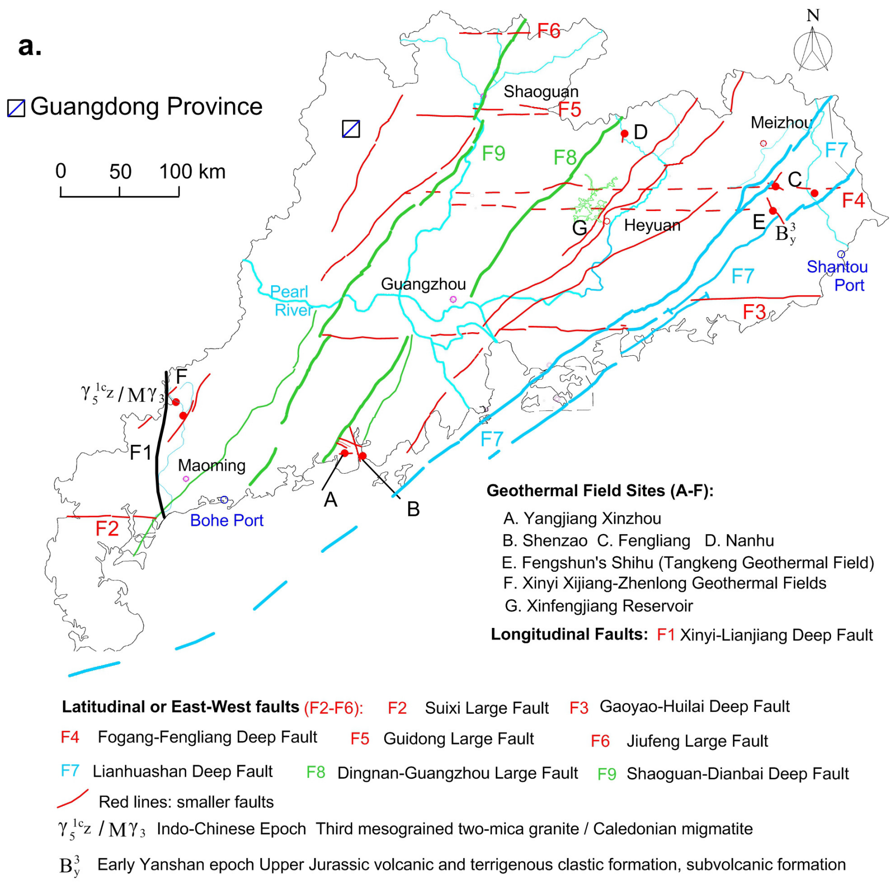

Hydrol. Earth Syst. Sci. Discuss., https://doi.org/10.5194/hess-2018-624
Manuscript under review for journal Hydrol. Earth Syst. Sci.
Discussion started: 8 February 2019

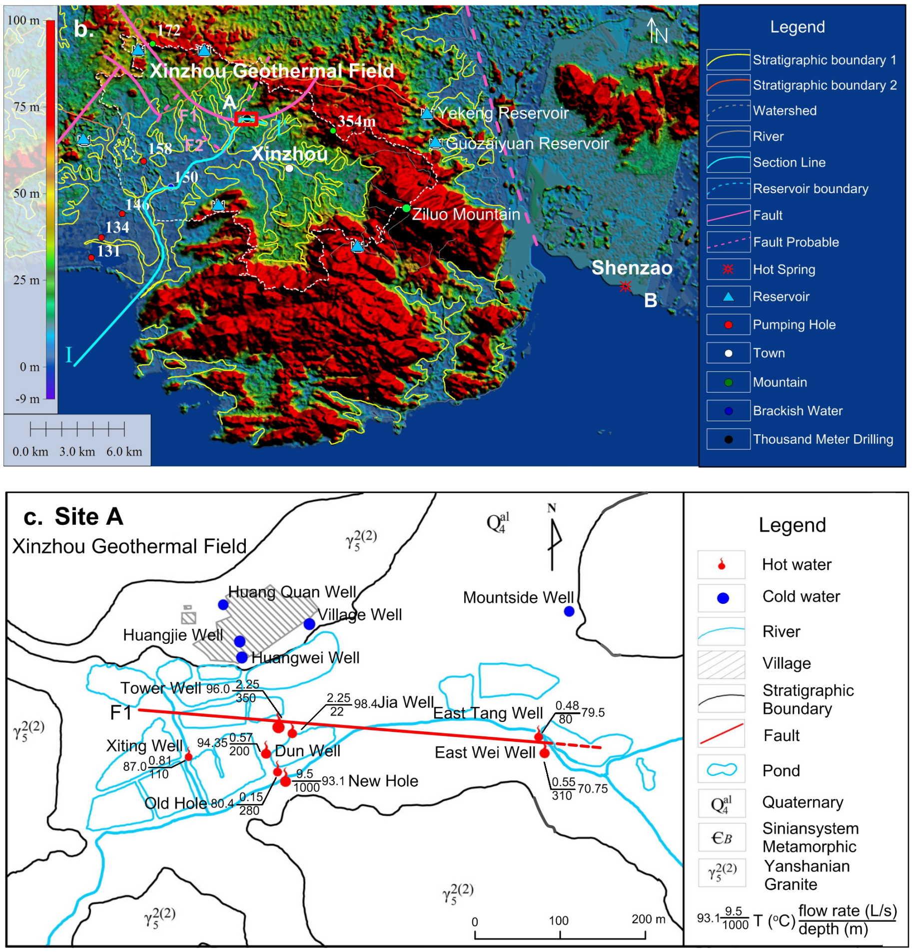

Figure 1. Geological background map for Xinzhou geothermal field in Yangjiang, Guangdong province: a. Regional tectonic map (Guangdong Province Geological Bureau Regional Geological Survey Brigade 1988; Chinese Academy of Sciences,1959); b. Regional geological map for Xinzhou geothermal field (Geological information drawn from 1: 250,000 outline configuration diagram of Yangjiang city, 2004); and c. Water sampling sites. New Hole was a 1000 m deep scientific borehole (Wang et al., 2015). Cross section I-I' shown the local stream discharge.

Hydrol. Earth Syst. Sci. Discuss., https://doi.org/10.5194/hess-2018-624
Manuscript under review for journal Hydrol. Earth Syst. Sci.
Discussion started: 8 February 2019

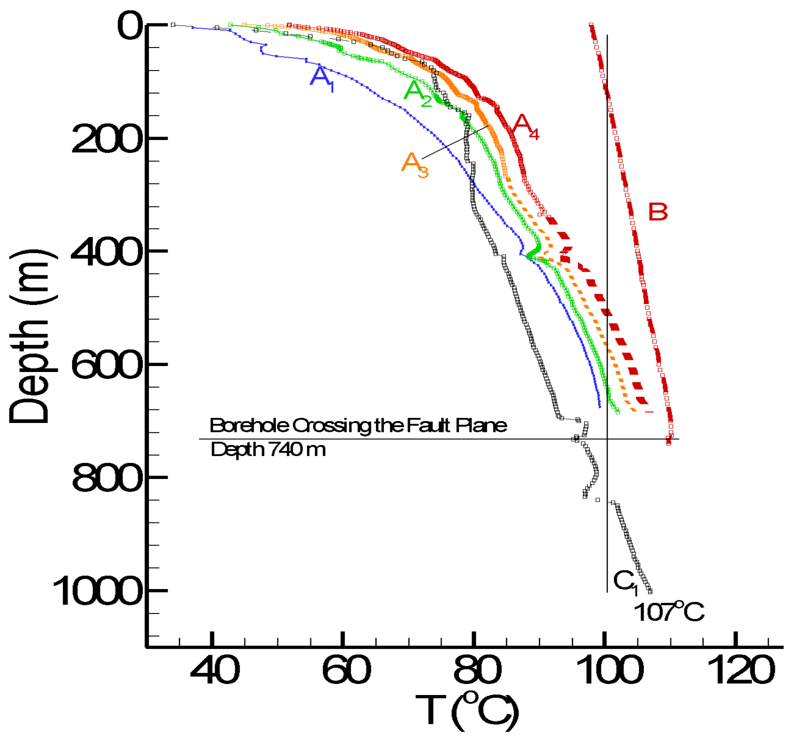

Figure 2. Temperature profiles during drilling of the 1000 m borehole (Figure 1c). A: curves for temperature recovery at the 685 m drilling depth, with A1, A2, A3 measurements from Oct. 30, 31 to Nov.1, 2, 2013. A4: Curve prior to thermal water eruption at 740 m depth, on Nov.7, 2013. B: Curve at the thermal water eruption at 740 m depth, on Nov.7, 2013, with 109.8°C recorded at 740 m. C: curve measured on Dec. 7, 2013 for final drilling depth 1002.25 m. Relevant statistic data in Tables 2 and 3

Hydrol. Earth Syst. Sci. Discuss., https://doi.org/10.5194/hess-2018-624
Manuscript under review for journal Hydrol. Earth Syst. Sci.
Discussion started: 8 February 2019

Hydrology and Earth System Sciences
Discussions
Open Access

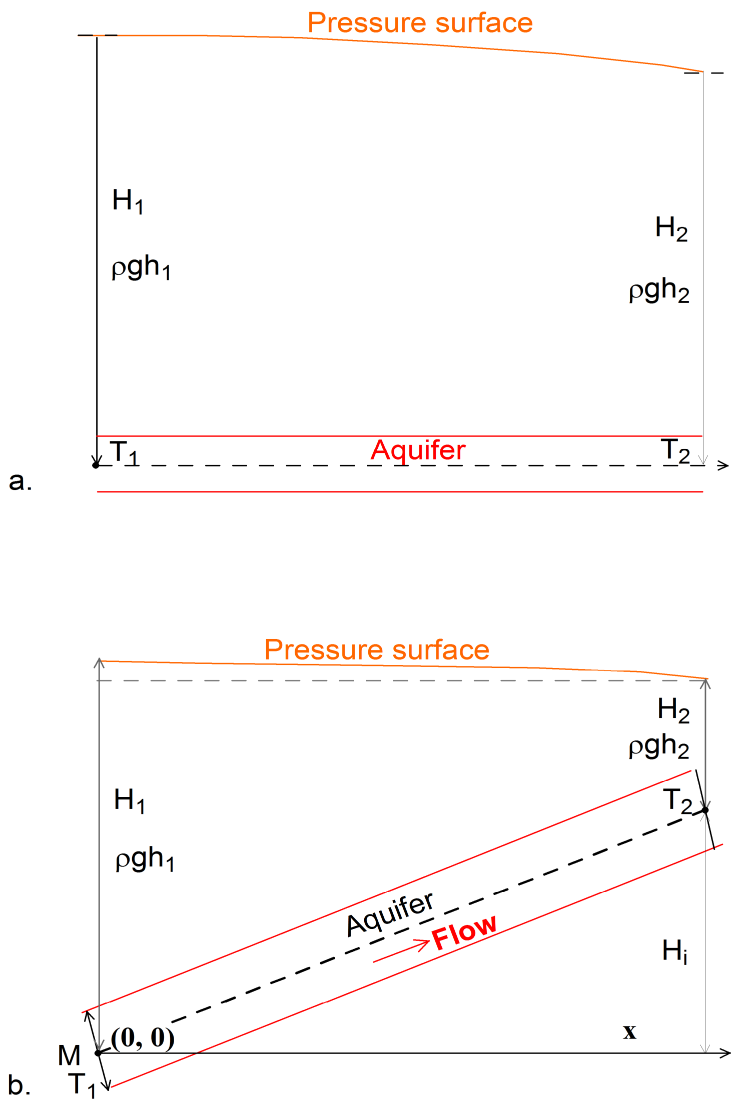

Figure 3. Geothermal water flow in confined aquifer under non-isothermal conditions. a. Horizontal aquifer under no flow condition; b. Inclined aquifer. The origin of the coordinates goes through the center point of the aquifer.

Hydrol. Earth Syst. Sci. Discuss., https://doi.org/10.5194/hess-2018-624
Manuscript under review for journal Hydrol. Earth Syst. Sci.
Discussion started: 8 February 2019

Hydrology and Earth System Sciences
Open Access
Discussions

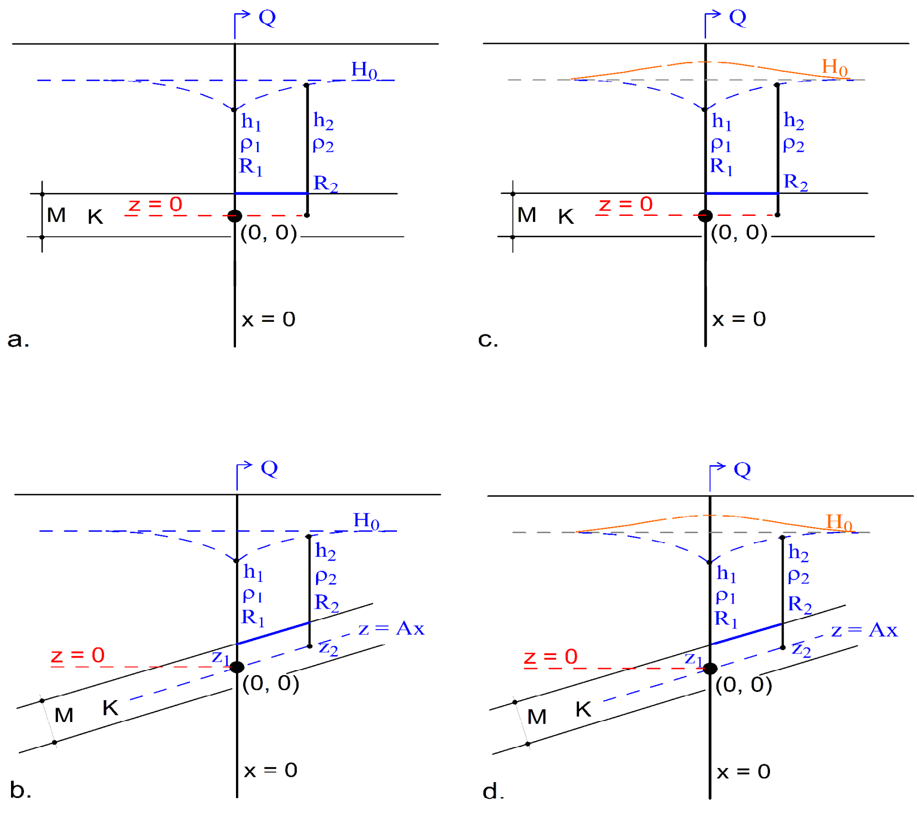

Figure 4. Illustration of an inclined confined aquifer under isothermal and non-isothermal conditions. a. Isothermal horizontal aquifer; b. Isothermal inclined aquifer; c. Non isothermal horizontal aquifer, and d. Non isothermal inclined aquifer. The origin of the coordinates goes through the well at the center point of the aquifer. where z = Ax is the median line through reference origin (0, 0) with A as the slope.

Hydrol. Earth Syst. Sci. Discuss., https://doi.org/10.5194/hess-2018-624
Manuscript under review for journal Hydrol. Earth Syst. Sci.
Discussion started: 8 February 2019

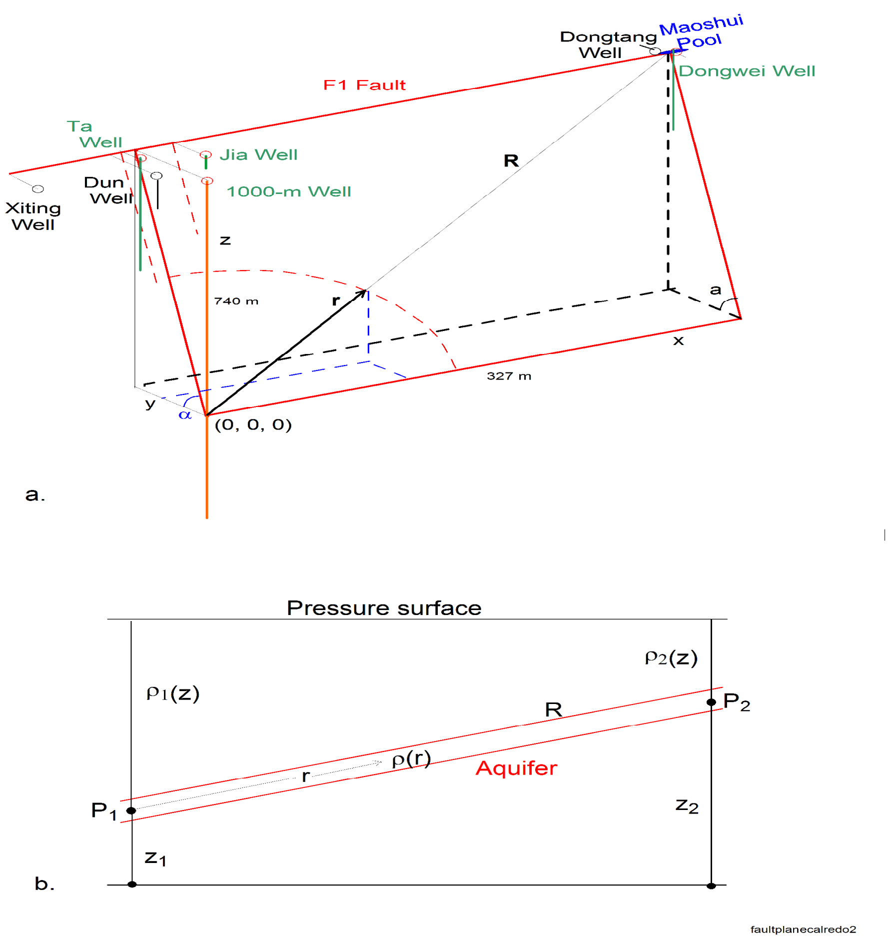

Figure 5. Illustration of deep fault F1 in Xinzhou geothermal field. a. The F1 fault plane; b. Well borehole system. α is the dip angle of the deep fault F1 at 85°, y-axis points to the foot wall along the deepest gradient, and x axis the horizontal along the strike of the fault plane. Location of the fault is referred to Figure 1c.